

1
2
3
4
5
6
7
8
9
10
11
12
13
14
15
16
17
18
19
20

Demonstrating frequency-dependent transmission of sarcoptic mange in red foxes

Eleanor S. Devenish-Nelson¹, Shane A. Richards¹, Stephen Harris², Carl Soulsbury³, Philip A. Stephens¹

¹School of Biological and Biomedical Sciences, Durham University, Durham, DH1 3LE, United Kingdom.

²School of Biological Sciences, University of Bristol, Bristol, BS8 1TQ, United Kingdom.

³School of Life Sciences, University of Lincoln, Lincoln, LN6 7TS, United Kingdom.

† Corresponding author: e.s.nelson@dunelm.org.uk

21 **Summary**

22 Understanding the relationship between disease transmission and host density is essential for
23 predicting disease spread and control. Using long-term data on sarcoptic mange in a red fox
24 *Vulpes vulpes* population, we tested long-held assumptions of density- and frequency-
25 dependent direct disease transmission. We also assessed the role of indirect transmission.
26 Contrary to assumptions typical of epidemiological models, mange dynamics are better
27 explained by frequency-dependent disease transmission than by density-dependent
28 transmission in this canid. We found no support for indirect transmission. We present the first
29 estimates of R_0 and age-specific transmission coefficients for mange in foxes. These
30 parameters are important for managing this poorly understood but highly contagious and
31 economically damaging disease.

32

33 **Keywords:** Age-specific infection, basic reproductive number, frequency-dependent
34 transmission, indirect transmission, SEI model.

35 **Introduction**

36 Rates of disease transmission are typically assumed to increase with host density for
37 most directly transmitted infections but to be unrelated to density for sexually and indirectly
38 transmitted diseases [1]. Increasingly, studies are challenging this assumption, suggesting that
39 behaviours mediating contact rates do not always show simple relationships with host density
40 [2]. Many diseases are also transmitted indirectly through contact with contaminated
41 substances known as fomites, a pathway only recently incorporated into wildlife disease
42 models [3, 4]. Insight into pathogen spread is informative for controlling disease: non-linear
43 dynamics can result in ineffective culling [5]; disease-induced extinction risk increases when
44 transmission is density-independent [6]; and indirect transmission can promote disease
45 persistence [3]. Given the threat of emerging infectious diseases, the possibility of domestic-
46 wildlife cross-infection and the cost of disease control [7, 8], understanding transmission
47 mechanisms is clearly important.

48 Sarcoptic mange, caused by the highly contagious mite *Sarcoptes scabiei*, affects over
49 100 domestic and wild mammalian species [9]. Mange is a potential emerging disease [7],
50 posing a risk for endangered species and domestic-wildlife infection [8]. The economic costs
51 of controlling mange are substantial [10]. Despite its importance, fundamental aspects of
52 mange epidemiology, including genetic resistance and transmission dynamics in wild
53 populations, are poorly understood [9]. Further, mange occurs in a range of species exhibiting
54 different levels of sociality [11-14].

55 Mange epizootics have caused significant declines in red fox *Vulpes vulpes*
56 populations worldwide [11, 15, 16]. Previous mange models have only considered direct,
57 density-dependent transmission [12, 17] but off-host mite survival [9] and low inter-group
58 contact in foxes [18] suggest that indirect transmission is likely. Moreover, the social nature
59 of foxes suggests that the traditional assumptions of density- and frequency-dependent
60 disease transmission might be complicated [19]. We developed a model of mange spread and
61 fitted it to a long-term dataset. This model allowed us to: (i) estimate epidemiological
62 parameters; (ii) explore whether transmission is frequency- or density-dependent; and (iii)
63 assess the potential role of indirect transmission.

64

65 **Methods**

66 An urban fox population in Bristol, UK, experienced a mange epizootic [20], followed by an
67 enzootic phase [11], during a four-decade long study (1977 to present). Pre-epizootic spring
68 population density (adults and juveniles) was exceptionally high (58.3 individuals km⁻²) and

69 post-epizootic density was reduced by >95% [20]. Monthly mange prevalence was
70 determined for juveniles (<1 year old) and adults (>1 year old), given observed age-related
71 patterns (see electronic supplementary material (ESM) for full details).

72 Using an age-structured Susceptible-Exposed-Infected (SEI) model, we tested two
73 forms of direct transmission: density- and frequency-dependent transmission (M_D and M_F ,
74 respectively, Figure 1) (see ESM for full model details). Two epidemiological parameters, the
75 transmission coefficient, β , and infectious period, γ , were estimated by fitting the models to
76 data. To account for potential age-specific variation in prevalence between juveniles (j) and
77 adults (a), the SEI model included age-specific transmission, denoted by the coefficients β_{jj}
78 and β_{aa} . The exposed class was included to incorporate the time taken between foxes
79 becoming exposed to the mites and becoming infectious, typically 30 days (Table 1). Mean
80 time to disease-induced mortality (α) is estimated to be 100 days (Table 1) which, with a life-
81 expectancy without the disease of 2 years, translates to a 7-fold increase in mortality rate due
82 to mange. Recovered individuals were assumed to return directly to the susceptible class
83 because re-infection of individuals was observed (S. Harris *unpublished data*). Host
84 demography was modelled assuming a fixed background *per capita* mortality rate (Table 1)
85 and an annual birth pulse. The total population density (N) was reset annually to an observed
86 post-breeding density (N_k), to simulate the birth pulse, with susceptible juveniles (S_{bj})
87 introduced into the population each year, t (i.e. $S_{bj} = N_k(t) - N$).

88 In models M_{DI} and M_{FI} , indirect transmission was combined with direct transmission
89 (Figure 1), given that indirect pathways are unlikely to be the sole transmission mechanism.
90 An additional compartment (F) followed mite density on fomites and the transmission
91 coefficient, β_f , described infection through the contact of susceptible individuals with free-
92 living mites on infected substrates. Due to paucity of data, the rate that mites are released into
93 the environment, ω , was a fitted parameter, assumed to depend on the reproductive rate of the
94 mites and individual parasite loads.

95 Parameter estimates were determined using maximum likelihood (see ESM for full
96 methods) in R 3.1.0 (www.r-project.org). Where possible, initial parameter values were
97 estimated from the literature [11, 20, 21] (Table 1). To determine the performance of the
98 disease transmission models, predicted dynamics were compared with a null model with
99 time-invariant disease prevalence. Evidence for inter-annual variation in post-breeding
100 density, density- versus frequency-dependent transmission, and the role of indirect
101 transmission were assessed by performing model selection using Akaike's Information
102 Criterion (AIC) [22]. The basic reproductive number, R_0 , determining the probability of

103 disease invasion, was calculated for the best AIC model using a ‘next generation matrix’ [23]
104 (see ESM).

105

106 **Results**

107 Age-related patterns in the monthly prevalence of mange (Figure S2) suggest some
108 seasonality, particularly in juveniles. Prevalence data were overdispersed with respect to the
109 binomial distribution (variance inflation factor, $\tilde{v} = 2.79$) and, therefore, all model likelihoods
110 were calculated using the beta-binomial distribution [22]. SEI models consistently
111 outperformed the null model (Table S1). AIC values for the null and all eight time-varying
112 disease models are presented in the ESM (Table S1). The most parsimonious models (M_F and
113 M_{FI}) indicated strong support for frequency-dependent mange transmission in the Bristol fox
114 population. The frequency-dependent model incorporating indirect transmission (M_{FI})
115 performed well but model comparison showed that the extra parameters did not justify the
116 increased complexity relative to model M_F (Figure 2a,b) [22]. M_F captured observed
117 prevalence patterns in both juveniles (Figure 2a) and adults (Figure 2b); the discrepancy
118 between empirical and observed juvenile prevalence from May to July is probably due to the
119 window of offspring birth being rather wider in reality than in our model. Density-dependent
120 models did not perform well (Figure 2c,d), overestimating juvenile prevalence from April to
121 June.

122 The 95% confidence intervals (CIs) of R_0 are all above one, consistent with mange
123 persistence in the population (Table 2). The best estimate of β'_{jj} was ten times higher than β'_{aa} ,
124 with no overlap between CIs (Table 2), suggesting a key role of juveniles for mange
125 transmission. The wide CIs and the discrepancy between the best model estimate of γ (Table
126 2, corresponding to 30 days) and the estimate from the literature [21], may reflect trade-offs
127 between γ and unknown parameters.

128

129 **Discussion**

130 This study presents the first published model of mange transmission dynamics in foxes. The
131 estimate of R_0 is consistent with mange invading the Bristol fox population and is similar in
132 magnitude to that estimated for mange in chamois *Rupicapra rupicapra* [$R_0=4.8-5.1$; 12].

133 In other fox populations, the relationship between mange and density is unclear [11,
134 15, 24]. However, contrary to expectation, frequency-dependent transmission of mange
135 appears most probable in the Bristol fox population, implying that the *per capita* rate of
136 infectious contact remains constant despite increases in densities of infected individuals. This

137 is consistent with fox behaviour, since opportunities for infectious contact may be limited due
138 to low inter- and intra-group encounters [18, 25]. Density-dependent models particularly
139 overestimated juvenile disease prevalence post-birth, when movement is limited. The
140 minimal effect of density on mange is supported by the observation that mange persists at
141 low fox densities [20], because frequency-dependent diseases can be sustained at lower host
142 densities than density-dependent diseases [26]. The contrast between our results and those of
143 assessments of mange transmission in chamois, a species which does not show complex
144 group structuring, and for which density-dependent transmission of mange was well-
145 supported [12], emphasises the role of sociality in mediating disease dynamics within a
146 population [1, 2, 5, 19]. Further work is needed to examine how transmission mechanisms
147 vary across different species affected by the same disease.

148 We found no support for indirect transmission. This could reflect the limited role of
149 this pathway between social groups in the study area: although inter-group den sharing
150 promoted mange transmission in a Russian fox population [16], this behaviour may be less
151 frequent in the Bristol population. Poor support for indirect transmission also suggests poor
152 support for the importance of alternative hosts. In single host – single pathogen models,
153 alternative hosts may appear to play a role equivalent to indirect transmission, especially
154 where the vectors are host generalists (as in the case of mange mites). However, in Bristol,
155 there was only evidence of mange transmission from foxes to dogs during the initial epizootic
156 phase, and no evidence of transmission from dogs to foxes (S. Harris *unpublished data*).
157 Thus, consistent with our findings on indirect transmission, the role of alternative hosts is
158 likely to be negligible. These findings should recognize, however, that population-level SEI
159 models do not discriminate between inter- and intra-group encounter rates and, thus, could
160 overestimate the importance of direct transmission between individuals of the focal species.
161 Simulations of individual-level behaviour may provide further insight into the relative
162 importance of transmission mechanisms.

163 The predicted age-specific prevalence may reflect the restricted post-birth movement
164 of juveniles [27] and the subsequent pulse of infection driven by the naïve source of
165 susceptible juveniles. The high predicted age-specific transmission rate suggests either that
166 juveniles are more prone to infection given contact (owing to less effective immune systems
167 and increased nutritional stress from independent foraging) and/or that they encounter
168 infected individuals more often than adults (owing to life-stage specific movement patterns);
169 however, combining data on all individuals younger than one may mask underlying
170 mechanisms. Mange is probably maintained by older individuals since adults have a longer

171 time to become infected compared to the short disease duration in younger individuals. Such
172 insight into age-specific transmission is important for disease control.

173 This study provides the first estimates of stage-dependent transmission rates and R_0
174 for mange in foxes and suggests that the dominant transmission mechanism is frequency-
175 dependent. These results indicate the importance of sociality in mange transmission and
176 highlight the need to test long-standing assumptions of disease transmission.

177

178 **Acknowledgements**

179 We thank Durham University and the Dulverton Trust for financial support, and the Durham
180 University Ecology Group for insightful discussions.

181

182 **References**

- 183 1. McCallum H., Barlow N., Hone J. 2001 How should pathogen transmission be
184 modelled? *Trends Ecol Evol* **16**, 295-300
- 185 2. Smith M.J., Telfer S., Kallio E.R., Burthe S., Cook A.R., Lambin X., Begon M. 2009
186 Host-pathogen time series data in wildlife support a transmission function between density
187 and frequency dependence. *Proc Natl Acad Sci USA* **106**, 7905-7909
- 188 3. Rohani P., Breban R., Stallknecht D.E., Drake J.M. 2009 Environmental transmission
189 of low pathogenicity avian influenza viruses and its implications for pathogen invasion. *Proc*
190 *Natl Acad Sci USA* **106**, 10365-10369
- 191 4. Miller M.W., Hobbs N.T., Taverer S.J. 2006 Dynamics of prion disease transmission
192 in mule deer. *Ecol Appl* **16**, 2208-2214
- 193 5. Morters M.K., Restif O., Hampson K., Cleaveland S., Wood J.L.N., Conlan A.J.K.
194 2013 Evidence-based control of canine rabies: a critical review of population density
195 reduction. *J Anim Ecol* **82**, 6-14
- 196 6. McCallum H., Jones M., Hawkins C., Hamede R., Lachish S., Sinn D.L., Beeton N.,
197 Lazenby B. 2009 Transmission dynamics of Tasmanian devil facial tumor disease may lead
198 to disease-induced extinction. *Ecology* **90**, 3379-3392
- 199 7. Daszak P., Cunningham A.A., Hyatt A.D. 2000 Emerging infectious diseases of
200 wildlife - threats to biodiversity and human health. *Science* **287**, 443-449

- 201 8. Smith K.F., Acevedo-Whitehouse K., Pedersen A.B. 2009 The role of infectious
202 diseases in biological conservation. *Anim Conserv* **12**, 1-12.(10.1111/j.1469-
203 1795.2008.00228.x)
- 204 9. Pence D.B., Ueckermann E. 2002 Sarcoptic mange in wildlife. *Rev Sci Tech Off Int*
205 *Epizoot* **21**, 385-398
- 206 10. Dobson K.J., Cargill C.F. 1980 Epidemiology and economic consequence of sarcoptic
207 mange in pigs. *Proceedings of the 2nd International Symposium on Veterinary Epidemiology*
208 *and Economics*, International Symposia on Veterinary Epidemiology and Economics ISVEE
209 May 1979, 401-407 International Symposia on Veterinary Epidemiology and Economics
- 210 11. Soulsbury C.D., Iossa G., Baker P.J., Cole N.C., Funk S.M., Harris S. 2007 The
211 impact of sarcoptic mange *Sarcoptes scabiei* on the British fox *Vulpes vulpes* population.
212 *Mammal Rev* **37**, 278-296.(10.1111/j.1365-2907.2007.00101.x)
- 213 12. Lunelli A. 2010 An SEI model for sarcoptic mange among chamois. *J Biol Dyn* **4**, 140
214 - 157
- 215 13. Graczyk T.K., Mudakikwa A.B., Cranfield M.R., Eilenberger U. 2001 Hyperkeratotic
216 mange caused by *Sarcoptes scabiei* (Acariformes : Sarcoptidae) in juvenile human-habituated
217 mountain gorillas (*Gorilla gorilla beringei*). *Parasitol Res* **87**, 1024-1028
- 218 14. Kołodziej-Sobocińska M., Zalewski A., Kowalczyk R. 2014 Sarcoptic mange
219 vulnerability in carnivores of the Białowieża Primeval Forest, Poland: underlying
220 determinant factors. *Ecol Res* **29**, 237-244
- 221 15. Lindström E., Morner T. 1985 The spreading of sarcoptic mange among Swedish red
222 foxes (*Vulpes vulpes* L) in relation to fox population dynamics. *Rev Ecol Terr Vie* **40**, 211-
223 216
- 224 16. Gerasimoff Y.A. 1958 Mange in wild foxes. Translation of Russian game reports
225 Volume 3 (arctic and red foxes, 1951-55), 70-85. *Canadian Department of Northern Affairs*
226 *and National Resources, Ottawa,*
- 227 17. Leung B., Grenfell B.T. 2003 A spatial stochastic model simulating a scabies
228 epidemic and coyote population dynamics. *Ecol Model* **166**, 41-52.(10.1016/s0304-
229 3800(03)00117-0)

- 230 18. White P.C.L., Harris S. 1994 Encounters between red foxes (*Vulpes vulpes*) -
231 implications for territory maintenance, social cohesion and dispersal. *J Anim Ecol* **63**, 315-
232 327
- 233 19. Sterner R.T., Smith G.C. 2006 Modelling wildlife rabies: transmission, economics,
234 and conservation. *Biol Conserv* **131**, 163-179.(10.1016/j.biocon.2006.05.004)
- 235 20. Baker P.J., Funk S.M., Harris S., White P.C.L. 2000 Flexible spatial organization of
236 urban foxes, *Vulpes vulpes*, before and during an outbreak of sarcoptic mange. *Anim Behav*
237 **59**, 127-146
- 238 21. Newman T.J., Baker P.J., Harris S. 2002 Nutritional condition and survival of red
239 foxes with sarcoptic mange. *Can J Zool* **80**, 154-161.(10.1139/z01-216)
- 240 22. Richards S.A. 2008 Dealing with overdispersed count data in applied ecology. *J Appl*
241 *Ecol* **45**, 218-227
- 242 23. Diekmann O., Heesterbeek J.A.P., Roberts M.G. 2010 The construction of next-
243 generation matrices for compartmental epidemic models. *J Royal Soc Interface* **7**, 873-885
- 244 24. Gortázar C., Villafuerte R., Blanco J.C., Fernández-De-Luco D. 1998 Enzootic
245 sarcoptic mange in red foxes in Spain. *Z Jagdwiss* **44**, 251-256
- 246 25. Giuggioli L., Potts J.R., Harris S. 2011 Animal interactions and the emergence of
247 territoriality. *PLoS Comp Biol* **7**, e1002008.(10.1371/journal.pcbi.1002008)
- 248 26. Ryder J.J., Miller M.R., White A., Knell R.J., Boots M. 2007 Host-parasite population
249 dynamics under combined frequency- and density-dependent transmission. *Oikos* **116**, 2017-
250 2026.(10.1111/j.2007.0030-1299.15863.x)
- 251 27. Robertson C.P.J., Baker P.J., Harris S. 2000 Ranging behaviour of juvenile red foxes
252 and its implications for management. *Acta Theriol* **45**, 525-535

253

254

255 Table 1. Definition of fitted and fixed parameters used in SEI models.

256

<i>Parameter</i>	<i>Definition</i>	<i>Fixed or fitted parameter</i>
β_{jj}, β_{aa}	Age-specific density-dependent transmission (day^{-1})	a
β'_{jj}, β'_{aa}	Age-specific frequency-dependent transmission ($\text{individual}^{-1} \text{day}^{-1}$)	a
β_f	Indirect transmission (day^{-1} per unit of fomite) (age-invariant)	a
γ	Infectious period = $1/\gamma$ (day^{-1})	a
σ	Latent period = $1/\sigma$ (day^{-1})	30 days
α	Disease-induced mortality rate = $1/\alpha$ (day^{-1})	100 days
μ_j	Juvenile <i>per capita</i> mortality probability (year^{-1})	0.3 ^b
μ_a	Adult <i>per capita</i> mortality probability (year^{-1})	0.5 ^b
ω	<i>Per capita</i> reproductive rate of mite on infected individuals (day^{-1})	a
ε	Rate of loss of the pathogen in environment = $1/\varepsilon$ (day^{-1})	10 days
S_{0j}	Initial density of susceptible juveniles (km^{-2})	21
S_{0a}	Initial density of susceptible adults (km^{-2})	36
I_{0j}	Initial density of infected juveniles (km^{-2})	0.01
I_{0a}	Initial density of infected adults (km^{-2})	0.01
F_0	Initial density of fomites (normalised)	1

257

258 ^a Fitted parameter

259 ^bAnnual probabilities were converted to daily rates by $-\ln(\mu)/360$

260

261 Table 2. Estimated parameter values for the best-fitting model (95% CIs in parentheses
 262 estimated by bootstrapping 10,000 replicates, see ESM). See Table 1 for epidemiological
 263 parameter descriptions.

264

<i>Model</i>	β'_{jj}	β'_{aa}	γ	Φ^a	R_0
M _F Frequency-dependent	0.340 (0.164– 0.705)	0.030 (0.006– 0.151)	0.039 (0.029– 0.111)	0.247 (0.156– 0.392)	2.67 1.54 – 5.12)

265

266

267

^aDispersion parameter, ϕ , indicating that data are overdispersed.

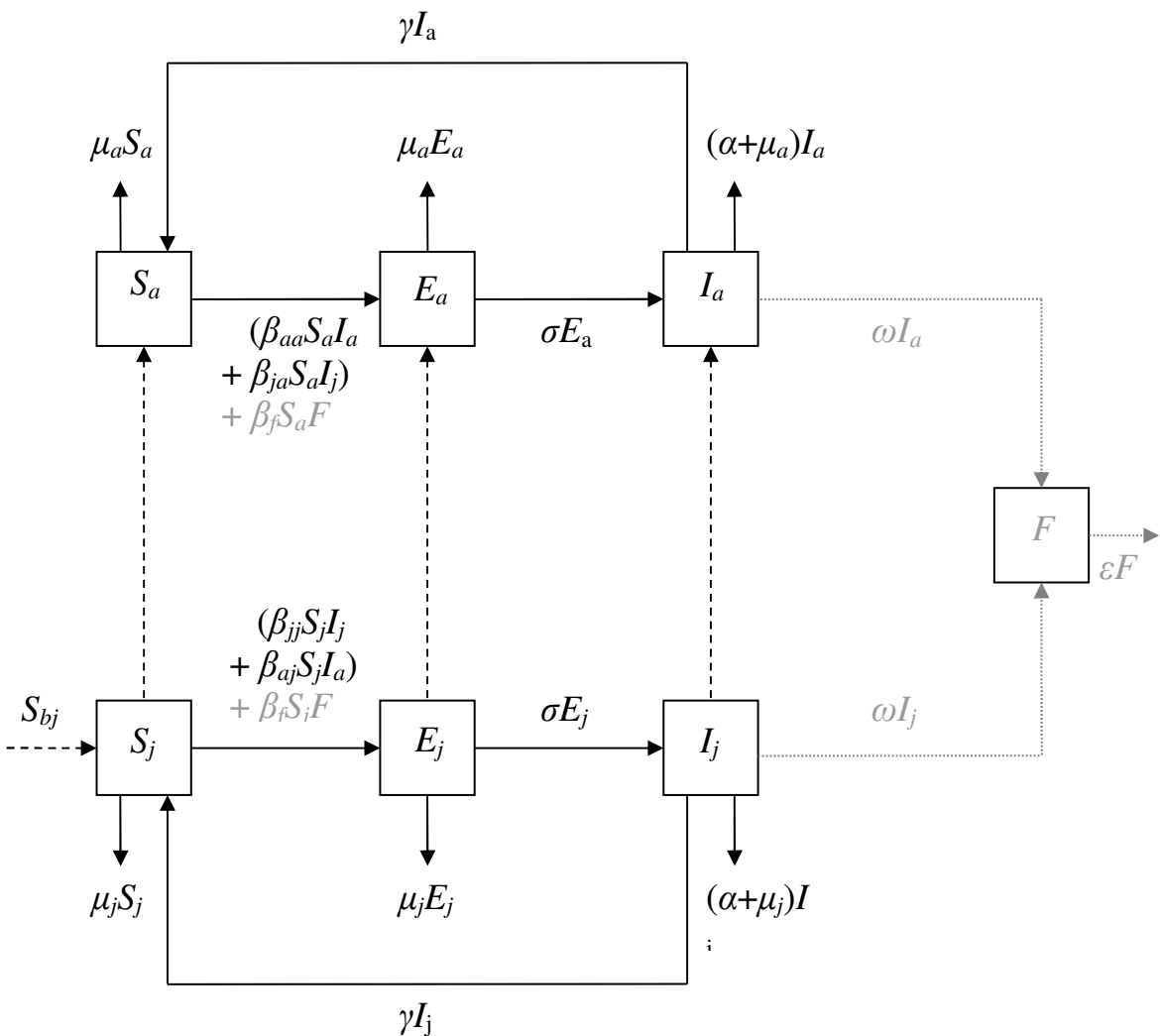
268 **Figure legends**

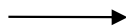

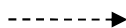
269

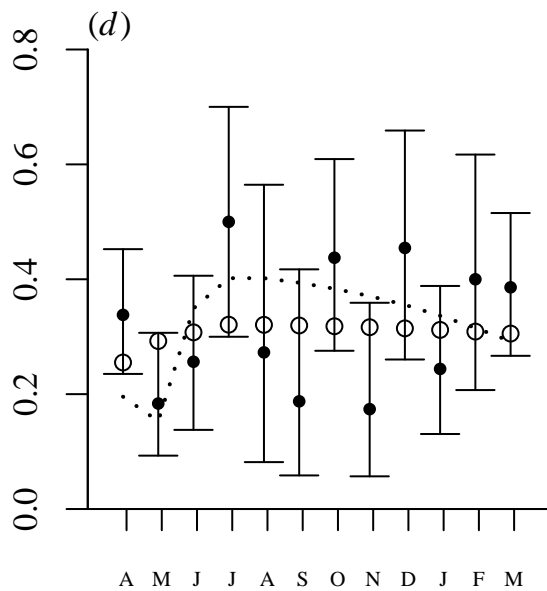
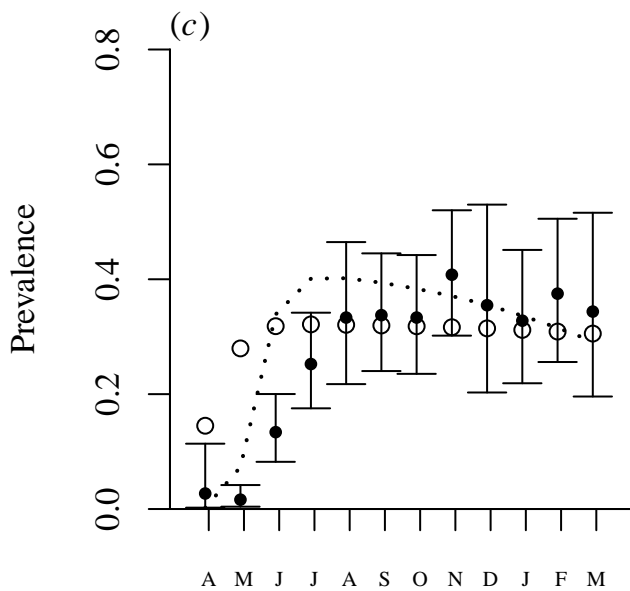
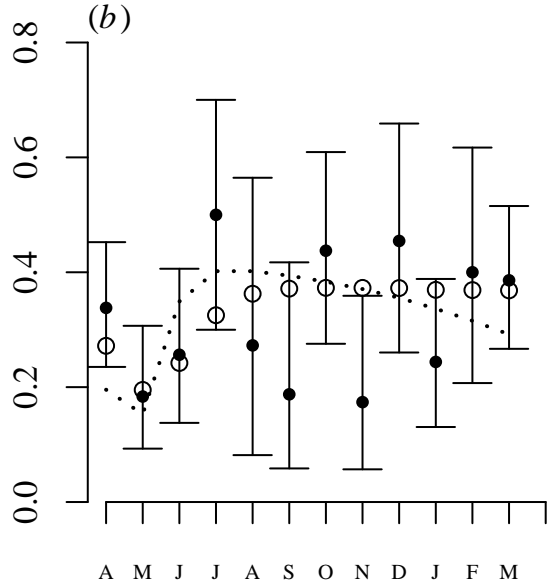
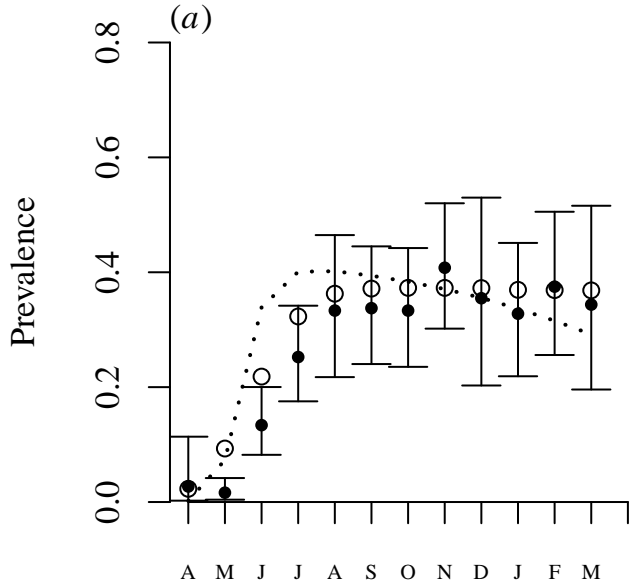
270 Figure 1. SEI compartment model diagram illustrating age-specific density-dependent direct
271 transmission with host demography (M_D). Indirect transmission and fomite dynamics are
272 indicated in grey (M_{DI}). Transmission terms in brackets are replaced with $(\beta'_{aa}S_aI_a +$
273 $\beta'_{ja}S_aI_j)/N$ and $(\beta'_{jj}S_jI_j + \beta'_{aj}S_jI_a)/N$ for frequency-dependent models (M_F and M_{FI}) (Table 1
274 provides parameter definitions).

275

276 Figure 2. The predicted probability of infection (open circles) for (a and b) the frequency-
277 dependent model (M_F), and for (c and d) the density-dependent model (M_D), for juveniles
278 (left panels) and adults (right panel), against the observed prevalence data (closed circles).
279 Dotted lines indicate the predicted probability of infection for models including indirect
280 transmission (M_{FI} and M_{DI} , respectively). 95% CIs were calculated from likelihood profiles.



-  Infection and mortality
-  Fomite dynamics
-  Births and maturation



Month

Month

Electronic Supplementary material (ESM):

Demonstrating frequency-dependent transmission of sarcoptic mange in red foxes

E. S. Devenish-Nelson, S. A. Richards, S. Harris, C. Soulsbury, P. A. Stephens

ESM 1.1: Data

In the UK, the Bristol fox population experienced a sarcoptic mange epizootic from 1994 to 1996; prevalence peaked in the autumn of 1995 when it was estimated that close to 100% of the population was infected [1]. At the start of the epizooty, the total (adults i.e. animals >1 year old and juveniles i.e. animals <1 year old) fox population density was 58.3 individuals km⁻²; this declined by >95% by the end of 1996 [1]. Population recovery was slow and mange has remained at enzootic levels since 1996 [2]; by 2014, prevalence levels were very low (S. Harris *unpublished data*). Annual post-breeding population densities [3, 4], were estimated from capture-mark-recapture data [e.g. 1]. Four years with missing estimates (1996, 1997, 2000, 2001) were determined by linear interpolation.

Prevalence and mortality data used in this analysis were based on data collected from a 14km² area of suburban Bristol through the recapture of radio-collared or marked individuals, and recovery of fox carcasses, from 1994 to 2010 (n=1662 records; S. Harris *unpublished data*) [sampling protocols are described in 2, 5]. Mange diagnosis was classified according to the disease manifestation [for a review of clinical symptoms see 6]; class I and class II infections were defined as no evidence of, and presence of, hyperkeratotic mange, respectively [see 5]. Due to the small monthly sample sizes, class I and class II data were combined to obtain the number of infected individuals per month. Monthly prevalence was then calculated as the proportion of infected juveniles and adults respectively. Prevalence data were not sufficiently detailed to add a pre-emergent age class. To determine uncertainty in the prevalence data, 95% confidence intervals were calculated from likelihood profiles.

Mean monthly sample sizes for adults (2.61, SD \pm 0.79, n = 502) and juveniles (5.53, SD \pm 1.30, n =1061) were consistent during the year (Figure S1), with the exception of a peak in juvenile capture and mortality records in the summer months, which reflects the newly mobile juveniles (Figure S1A). Juveniles were sampled (Figure S1A), on average, twice as frequently as adults (**Error! Reference source not found.**Figure S1B), reflecting the age distribution of the population. Mean sample sizes of infected individuals for monthly prevalence data were low for both age classes (adults 0.63, SD \pm 0.28, n = 120; juveniles 0.99, SD \pm 0.33, n = 191; Figure S2). Age-related patterns in the monthly prevalence of mange (Figure S2) suggest some seasonality, particularly in juveniles. Confidence intervals are wide, however, indicating substantial uncertainty in the data.

ESM 1.2: SEI models

Although *S. scabiei* is conventionally classified as a macroparasite, because it displays several microparasite attributes (the small mites reproduce directly and rapidly on the host and are able to transfer directly between host individuals), a microparasite modelling approach was applied in this study to estimate the epidemiological parameters, β and γ , and compare pathways of mange transmission in foxes. An SEI model was used in which densities (N) of individuals in a given population are categorised into classes according to their disease status as susceptible (S), exposed (E), and infected (I) (i.e. $N = S + E + I$) (Figure 1). Two forms of direct transmission were modelled. Density-dependent transmission was the first direct mechanism modelled (M_D). Here, the transmission rate is proportional to the densities of both susceptible and infected groups within the population (βSI), resulting in prevalence increasing linearly with the density of these two groups. The second mode of direct transmission, frequency-dependent (M_F), assumes that the infection rate is dependent on the proportion of infective individuals in the population ($\beta' SI/N$); thus, opportunities for contact between an infectious and susceptible individual are assumed to be independent of population size [7].

Given that indirect pathways are unlikely to be the sole transmission mechanism of mange, Models M_{DI} and M_{FI} include both indirect transmission and direct transmission, with an additional compartment (F) following the densities of mites in the environment [8] (Figure 1). For analytical tractability, it was assumed that β_f was not age-specific. Under average ambient conditions, all life stages of the mite can survive an average of 10 days off the host, but this can increase to several weeks if conditions are optimal [6]. The parameter ω , the rate that mites are released into the environment, had to be fitted because, although it is known that female mites produce 3-4 eggs per day, with an average life expectancy of 5 weeks [9], parasite loads and the rate at which mites are released from the host remain undetermined.

Foxes breed annually and, for modelling purposes, it was assumed that all juveniles are born on April 1st (Harris & Smith 1987). Thus, for convenience, the total population density was reset annually to a post-breeding density (N_k), occurring in March because this process was modelled at the end of the month. In this way, a pulse of new susceptible individuals (S_{bj}) was introduced into the population each year ($S_{bj} = N_k(t) - N$). The post-breeding density $N_k(t)$ was defined as the total (combined juvenile and adult) population density estimate for year t , based on an independent set of density data (S. Harris *unpublished data*).

To account for potential age-specific variation in prevalence, for both density- and frequency-dependent transmission, a “Who Acquires Infection From Whom” (WAIFM) transmission matrix

[10] was used to denote transmission from one class to another, e.g. for frequency-dependent transmission:

$$\beta' = \begin{pmatrix} \beta'_{jj} & \beta'_{aj} \\ \beta'_{ja} & \beta'_{aa} \end{pmatrix}, \quad (\text{S1})$$

where j and a represent juveniles and adults respectively and β' is the frequency-dependent transmission coefficient. To reduce uncertainty in parameter estimates and to maintain analytical tractability, and because the addition of more complex contact rates was not supported by the data, it was assumed that juvenile-adult transmission, β'_{ja} , was equal to juvenile-juvenile transmission, β'_{jj} , and that adult-juvenile transmission, β'_{aj} , equalled adult-adult transmission, β'_{aa} . Each year, at the time of the birth pulse, juveniles in a given disease state matured into adults of the corresponding disease class. The following ordinary differential equations (ODEs) describe disease dynamics between birth pulses according to the frequency-dependent SEI model (M_F):

$$\begin{aligned} \frac{dS_j}{dt} &= -\mu_j S_j - (\beta'_{jj} I_j + \beta'_{aj} I_a) \frac{S_j}{N} + \gamma I_j \\ \frac{dE_j}{dt} &= -\mu_j E_j - \sigma E_{j+} (\beta'_{jj} I_j + \beta'_{aj} I_a) \frac{S_j}{N} \\ \frac{dI_j}{dt} &= -(\alpha + \mu_j) I_j + \sigma E_j - \gamma I_j \\ \frac{dS_a}{dt} &= -\mu_a S_a - (\beta'_{aa} I_a + \beta'_{ja} I_j) \frac{S_a}{N} + \gamma I_a \\ \frac{dE_a}{dt} &= -\mu_a E_a - \sigma E_{a+} (\beta'_{aa} I_a + \beta'_{ja} I_j) \frac{S_a}{N} \\ \frac{dI_a}{dt} &= -(\alpha + \mu_a) I_a + \sigma E_a - \gamma I_a, \end{aligned} \quad (\text{S2})$$

ESM 1.3: Parameter fitting and model selection

The SEI model parameters were fitted to the prevalence data using maximum likelihood. This analysis is based on the assumption that the transmission rate, β , of mange in a population, N , of S susceptible individuals produces I infected individuals per day, given that E individuals were exposed to the mite and became infectious. The probability an individual in the population is infected, p , is given by I/N . Predictions of the model can be compared to empirical observations on the prevalence of infected individuals by considering the process of field data collection as a series of binomial trials. Let the months in the total time series be denoted by $[m = 1, 2, 3, \dots, D]$. Within a given month, each individual sampled can be considered as a trial, with the total number of

individuals sampled in each age class denoted n_x . Assuming that the probability of becoming infected, p_x , is uniform among individuals sampled of age x , the number of infected individuals within an age class, y_x , will follow a binomial distribution. Thus, the likelihood at time m that proportion p_x of either juveniles or adults in the population are infected, given that a random sample of n_x individuals includes y_x infectives, is:

$$L(p_x | n_x, y_x) = \binom{n_x}{y_x} p_x^{y_x} (1 - p_x)^{n_x - y_x}. \quad (\text{S3})$$

Observed variation in the rate of infection can arise as a result of sampling error, including undiagnosed or misdiagnosed cases, or due to the effects of unmeasured factors such as individual variation in parasite load or susceptibility. If these sources of variation are unaccounted for and result in overdispersed data, then unnecessarily complex models can be selected when using information theoretic approaches because model precision will be overestimated [11, 12]. To measure the degree of dispersion in the data, the variance inflation factor, \tilde{v} , was estimated by dividing the variation in the observed data (saturated model, where the number of parameters equals the number of observations) by the variation in the most complex binomial model [11]. If overdispersion is present ($\tilde{v} \geq 2$), a compound distribution can be fitted to the data instead [11]. For binomial data, an appropriate compound distribution is the beta-binomial distribution. This model assumes that variation in p_x across samples within a given time period is described by the beta distribution:

$$f(p_x; \bar{p}_x, \phi) = \frac{\Gamma(a+b)}{\Gamma(a)\Gamma(b)} p_x^{a-1} (1 - p_x)^{b-1}, \quad (\text{S4})$$

where the parameter ϕ quantifies the variation in p_x , \bar{p}_x is the mean probability of success, $\Gamma(x)$ is the complete gamma function, $a = \bar{p}_x / \phi$, and $b = (1 - \bar{p}_x) / \phi$. Substituting equation (S4) into equation (S3) gives the compound beta-binomial distribution. If θ is the set of model parameters required to calculate \bar{p}_x and the dispersion coefficient ϕ , then the likelihood of θ at time m can be calculated as:

$$L(\theta | n_x, y_x) = \frac{\Gamma(n_x+1)\Gamma(a+b)\Gamma(y_x+a)\Gamma(n_x-y_x+b)}{\Gamma(y_x+1)\Gamma(n_x-y_x+1)\Gamma(a)\Gamma(b)\Gamma(n_x+a+b)}. \quad (\text{S5})$$

Equation (S4) approximates the binomial distribution as the dispersion parameter, ϕ , approaches zero. The total log-likelihood of the model, defined by θ and given all the data, is then the log of equation (S5) summed over age classes j and a over the total time period, D :

$$LL(\theta | \text{data}) = \sum_{m=1}^D \left\{ \sum_{j=1}^{n_j} (\ln L[\theta | n_{jm}, y_{jm}]) + \sum_{a=1}^{n_a} (\ln L[\theta | n_{am}, y_{am}]) \right\}. \quad (\text{S6})$$

To determine the ability of the disease transmission model to fit the data, it is useful to compare predicted dynamics with a null model in which disease prevalence is constant in time. A beta-binomial null model (M_H) was fitted which simply assumed that the probability a sampled individual in each age class was diseased was, on average, time-invariant ($p_x = \bar{p}_x$). The ability of SEI models to capture patterns in the prevalence data was determined by comparing the likelihoods of the null model, M_H , and those models that included disease parameters (M_D, M_F, M_{DI}, M_{FI}).

In general, it is necessary to use a discrete approximation because epidemiological ODE models cannot be solved analytically due to their non-linear properties. Thus, to obtain prevalence patterns, $p_x(m)$, predicted by each SEI model, the associated system of equations (eqn S2) was solved using the fourth-order Runge-Kutta method [13]. The set of model parameter values fitted to the monthly age-specific prevalence data for direct transmission were $\theta = \{\beta_{jj}, \beta_{aa}, \gamma, \varphi\}$ and $\theta = \{\beta'_{jj}, \beta'_{aa}, \gamma, \varphi\}$ for density- and frequency-dependent transmission respectively; for models that include indirect transmission, the models were defined by $\theta = \{\beta_{jj}, \beta_{aa}, \beta_f, \omega, \gamma, \varphi\}$ and $\theta = \{\beta'_{jj}, \beta'_{aa}, \beta_f, \omega, \gamma, \varphi\}$. Parameter estimates were determined by maximising the total model log-likelihood (eqn S6) using the “optim” function in R 3.1.0 (www.r-project.org). To distinguish between the competing models, Akaike’s Information Criterion (AIC) was used; to avoid instances where the best AIC model does not have the lowest AIC value due to uncertainty from sampling error, all models with $\Delta AIC \leq 6$ units were considered to have some level of support [11, 14]. A bootstrap approach was used to calculate 95% confidence intervals for each parameter of the best fitting model selected by AIC. Specifically, 1000 model replicates were fitted by re-sampling the prevalence data between years, but from the same month. All analyses were conducted in R 3.1.0 (www.r-project.org).

ESM 1.4: Basic Reproductive Number

1.4.1. Theoretical background

The basic reproductive number, R_0 , is defined as the expected number of secondary cases attributed to a typical infectious individuals in an entirely susceptible population [15]. Thus, in cases where $R_0 < 1$, a pathogen will not successfully invade when a typical infectious individual causes less than one infection in an entirely susceptible population. Such populations exhibit a stable disease-free equilibrium. When $R_0 > 1$, a pathogen will successfully invade causing instability in the disease-free equilibrium. In this regard, R_0 is a threshold parameter, reflecting whether a pathogen will successfully invade a population, describing the stability of a system’s disease-free equilibrium.

The above definition is acceptable in homogeneous populations and calculations of R_0 are well established for such models [15]. However, in heterogeneous populations, where infected individuals can be classified into discrete classes (e.g. by age or behaviour), defining a typical infectious individual is less straightforward, and estimating R_0 more complex [15-17]. Theoretically, in such cases, separate R_0 values for each class can be calculated; however, this does not provide a single value for estimating the likelihood of disease invasion in the entire population [10]. Further, averaging the individual R_0 values for each class to obtain a composite R_0 value leads to erroneous estimates, since it does not account for the proportion of infected individuals in each class. This can lead to R_0 being underestimated for heterogeneous populations [10]. Thus, it is necessary to account for the rate at which infection is transmitted between these heterogeneous classes by weighting R_0 according to the expected level of infection in each class in an entirely susceptible population [15].

In homogeneous compartment models, there are two dynamical phases of infection, whereas in heterogeneous models there are three phases. For a detailed description of these phases see [10]. The second phase in heterogeneous models is analogous to the stable stage distribution (SSD) of demographic models [18] and it is during this phase that an infection will successfully invade or die out. As with the SSD in demographic models [19], R_0 provides insight into the eventual growth rate of infection, while the growth of a disease in the early phase is independent of R_0 . In some instances, conditions favouring disease spread will change, and so R_0 may no longer be a suitable measure of disease transmission [17]. Nevertheless, R_0 continues to be a meaningful measure of disease spread since, in many disease systems, peak prevalence of infected hosts and the final size of an epidemic are increasing functions of R_0 [17].

In heterogeneous cases, R_0 is frequently determined using a ‘next generation matrix’ (NGM) [15-17, 20]. Here, the demographic equivalent of ‘being born’ into a ‘generation’ refers to ‘becoming infected’ [20]. R_0 is determined during the second dynamical phase, because this stage is independent of the initial conditions and presents a natural weighting of the number of infections caused by an initial infected individual, in each class [10].

In heterogeneous models, in order to find the next generation matrix, \mathbf{K} , it is necessary to consider infectious individuals of m distinct classes of which r are infected. $x = x_1, \dots, x_m$ is the density of individuals in compartment i and x_0 is the disease-free equilibrium. Since the relative change in susceptibles is small during the initial phase of invasion, their numbers can be fixed at the disease free equilibrium [20]. To calculate \mathbf{K} , two matrices need to be determined from the model; \mathbf{F} , which describes the rate at which new infections arise (gains) and \mathbf{V} , that describes the rate at which individuals enter or leave the infectious class due to infection, recovery or death (losses) [15].

Although there may be several ways to define \mathbf{F} and \mathbf{V} , there is usually only one that is biologically meaningful [21]. The rate of change of x_i is given by:

$$\frac{dx_i}{dt} = \mathbf{F}_i(x) - \mathbf{V}_i(x). \quad (\text{S7})$$

Here, $\mathbf{F}_i(x)$ is the rate of new infections in compartment i and $\mathbf{V}_i(x) = \mathbf{V}_i^-(x) - \mathbf{V}_i^+(x)$, where \mathbf{V}_i^+ describes the rate at which individuals enter compartment i , whilst \mathbf{V}_i^- describes the rate at which individuals leave the i th compartment.

In order to form the NGM, the following assumptions should be met [15, 21].

1. If a compartment contains no individuals, there can be no movement of individuals out of the compartment, through death, infection or other means.
2. No movement between compartments can be negative
3. If the population is disease-free, there can be no movement into the infectious population (e.g. through density-independent immigration of infectious individuals).
4. There can be no movement of infections into classes that are defined as non-infectious.
5. The disease-free equilibrium is locally asymptotically stable in the absence of new infections.

Assuming that these conditions are met, the NGM \mathbf{K} can then be formed from the partial derivatives of the matrices \mathbf{F}_i and \mathbf{V}_i , such that;

$$\mathbf{F} = \left[\frac{\partial F_i}{\partial x_s}(x_0) \right] \text{ and } \mathbf{V} = \left[\frac{\partial V_i}{\partial x_s}(x_0) \right], \quad (\text{S8, S9})$$

where $i, s = 1, \dots, r$. The (s,k) entry of \mathbf{V}^{-1} , describes the average length of time an infected individual introduced to compartment k spends in compartment s , and the (i,s) entry of \mathbf{F} is the rate at which an infectious individual in compartment s produces new infections in compartment i . The product of these matrices, \mathbf{FV}^{-1} , is the NGM \mathbf{K} . Thus, the (i,k) entry of \mathbf{FV}^{-1} provides the expected rate of new infections in compartment i produced by an infectious individual introduced to compartment k . When the matrix element $\mathbf{FV}_{i,k} = 0$, no new cases produced in infected state k can be in infected state i immediately following infection.

1.4.2. Calculating R_0

In the model described above (eqn S2), each age class has individuals in susceptible, exposed and infected disease compartments, such that the vector $x = (S_j, E_j, I_j, S_a, E_a, I_a)$ and the disease free equilibrium $x_0 = (S_j, 0, 0, S_a, 0, 0)$, with $S_j = S_{0j}$ and $S_a = S_{0a}$ defined as the initial densities. To define the NGM for this model, it is necessary to examine how new infections arise and how individuals move

between disease states. Since there are four infected states (E_j, E_a, I_j, I_a), the resulting system will be four-dimensional. To define the rate of new infections, evaluated at the disease-free equilibrium, the matrix \mathbf{F} was constructed for the above model as:

$$\mathbf{F} = \begin{bmatrix} 0 & 0 & \beta'_{jj} \frac{S_{0j}}{N} & \beta'_{aj} \frac{S_{0j}}{N} \\ 0 & 0 & \beta'_{ja} \frac{S_{0a}}{N} & \beta'_{aa} \frac{S_{0a}}{N} \\ 0 & 0 & 0 & 0 \\ 0 & 0 & 0 & 0 \end{bmatrix}. \quad (\text{S10})$$

To define how individuals can move between compartments, the matrix \mathbf{V} is:

$$\mathbf{V} = \begin{bmatrix} (\sigma + \mu_j) & 0 & 0 & 0 \\ 0 & (\sigma + \mu_a) & 0 & 0 \\ -\sigma & 0 & (\alpha + \mu_j + \gamma) & 0 \\ 0 & -\sigma & 0 & (\alpha + \mu_a + \gamma) \end{bmatrix}. \quad (\text{S11})$$

Since \mathbf{V} is a non-singular M-matrix [17], it can be inverted to obtain \mathbf{V}^{-1} :

$$\mathbf{V}^{-1} = \begin{bmatrix} \frac{1}{(\sigma + \mu_j)} & 0 & 0 & 0 \\ 0 & \frac{1}{(\sigma + \mu_a)} & 0 & 0 \\ \frac{\sigma}{(\sigma + \mu_j)(\alpha + \mu_j + \gamma)} & 0 & \frac{1}{(\alpha + \mu_j + \gamma)} & 0 \\ 0 & \frac{\sigma}{(\sigma + \mu_a)(\alpha + \mu_a + \gamma)} & 0 & \frac{1}{(\alpha + \mu_a + \gamma)} \end{bmatrix}. \quad (\text{S12})$$

These matrices are then multiplied to obtain:

$-\mathbf{FV}^{-1}$

$$= \begin{bmatrix} 0 & 0 & \beta'_{jj} \frac{S_{0j}}{N} & \beta'_{aj} \frac{S_{0j}}{N} \\ 0 & 0 & \beta'_{ja} \frac{S_{0a}}{N} & \beta'_{aa} \frac{S_{0a}}{N} \\ 0 & 0 & 0 & 0 \\ 0 & 0 & 0 & 0 \end{bmatrix} \begin{bmatrix} \frac{1}{(\sigma + \mu_j)} & 0 & 0 & 0 \\ 0 & \frac{1}{(\sigma + \mu_a)} & 0 & 0 \\ \frac{\sigma}{(\sigma + \mu_j)(\alpha + \mu_j + \gamma)} & 0 & \frac{1}{(\alpha + \mu_j + \gamma)} & 0 \\ 0 & \frac{\sigma}{(\sigma + \mu_a)(\alpha + \mu_a + \gamma)} & 0 & \frac{1}{(\alpha + \mu_a + \gamma)} \end{bmatrix}$$

$$= \begin{bmatrix} \frac{\sigma\beta'_{jj}}{(\sigma + \mu_j)(\alpha + \mu_j + \gamma)} \frac{S_{0j}}{N} & \frac{\sigma\beta'_{aj}}{(\sigma + \mu_a)(\alpha + \mu_a + \gamma)} \frac{S_{0j}}{N} & \frac{\beta'_{jj}}{\alpha + \mu_j + \gamma} \frac{S_{0j}}{N} & \frac{\beta'_{aj}}{\alpha + \mu_a + \gamma} \frac{S_{0j}}{N} \\ \frac{\sigma\beta'_{ja}}{(\sigma + \mu_j)(\alpha + \mu_j + \gamma)} \frac{S_{0a}}{N} & \frac{\sigma\beta'_{aa}}{(\sigma + \mu_a)(\alpha + \mu_a + \gamma)} \frac{S_{0a}}{N} & \frac{\beta'_{ja}}{\alpha + \mu_j + \gamma} \frac{S_{0a}}{N} & \frac{\beta'_{jj}}{\alpha + \mu_a + \gamma} \frac{S_{0a}}{N} \\ 0 & 0 & 0 & 0 \\ 0 & 0 & 0 & 0 \end{bmatrix}. \quad (S13)$$

However, of the four infected states, only two are ‘states-at-infection’, i.e. the state in which an individual becomes infected or has their ‘epidemiological birth’ [22]. In this model, E is the only state-at-infection, as an individual can only be in the state I after the latent period, not immediately after infection. NGM calculation relies only on the states-at-infection [22], which in this example are identified as the two non-zero rows of \mathbf{F} . Following established methods [22], \mathbf{FV}^{-1} is pre- and post-multiplied by an auxiliary matrix, \mathbf{E} , whose column elements relate to the non-zero rows of \mathbf{F} :

$$\mathbf{E} = \begin{bmatrix} 1 & 0 \\ 0 & 1 \\ 0 & 0 \\ 0 & 0 \end{bmatrix}. \quad (S14)$$

Hence, the next-generation matrix is:

$$\mathbf{K} = -\mathbf{E}'\mathbf{FV}^{-1}\mathbf{E} = \begin{bmatrix} \frac{\sigma\beta'_{jj}}{(\sigma + \mu_j)(\alpha + \mu_j + \gamma)} \frac{S_{0j}}{N} & \frac{\sigma\beta'_{aj}}{(\sigma + \mu_a)(\alpha + \mu_a + \gamma)} \frac{S_{0j}}{N} \\ \frac{\sigma\beta'_{ja}}{(\sigma + \mu_j)(\alpha + \mu_j + \gamma)} \frac{S_{0a}}{N} & \frac{\sigma\beta'_{aa}}{(\sigma + \mu_a)(\alpha + \mu_a + \gamma)} \frac{S_{0a}}{N} \end{bmatrix} \quad (S15)$$

Here, the epidemiological meaning of the elements is clear, where $\sigma/(\sigma + \mu)$ is the mean length of the latent period (i.e. probability of transitioning from infectious class E to I) and $1/(\alpha + \mu + \gamma)$ is the mean length of the infectious period (i.e. the probability of transitions out of the I infectious state).

The NGM is non-negative, such that the dominant eigenvalue is non-negative and, as shown previously [17], is a threshold parameter for the stability of the disease-free equilibrium. Associated with this eigenvalue is a non-negative eigenvector, w , that effectively describes the distribution of infected individuals that produce the greatest number, R_0 , of secondary infections per generation [21]. Thus R_0 and w together describe a ‘typical’ infectious individual, where R_0 is the spectral radius, ρ , or the dominant eigenvalue of the next-generation matrix:

$$R_0 = \rho(\mathbf{K}). \quad (S16)$$

For models including indirect transmission, the overall R_0 is equal to $R_0 + R_0^{indirect}$, where $R_0^{indirect}$ is calculated as [23]:

$$R_0^{indirect} = \frac{\omega\beta_f(S_{0j}+S_{0a})}{m(\mu+\alpha+\gamma)}. \quad (S17)$$

R_0 was calculated for the most parsimonious model selected by AIC, using the parameter value estimates obtained from maximum likelihood. To determine the 95% confidence intervals for R_0 , parameters values were resampled from a truncated multivariate normal distribution, using the mean and 95% confidence intervals from the model fitting process. CIs were then calculated for R_0 , from the 10,000 bootstrap replicates that were run using ‘rtmvnorm’ from the ‘tmvtnorm’ package in R 3.1.0 (www.r-project.org).

Table S1. Model selection results for null and SEI models. The number of parameters (K), log-likelihoods (LL), and AIC values for each model are presented. Parameters are defined in the Methods, and Table 1.

<i>Model</i>	<i>Parameters</i>	<i>K</i>	<i>Log-likelihood</i>	<i>AIC</i>	<i>ΔAIC</i>
M _H	Null model	3	-325.92	657.83	25.83
M _D	Density-dependent	4	-320.48	648.97	16.96
M _F	Frequency-dependent	4	-312.00	632.00	0
M _{DI}	Density-dependent + Indirect	6	-320.46	652.92	20.92
M _{FI}	Frequency-dependent + Indirect	6	-311.67	635.34	3.34

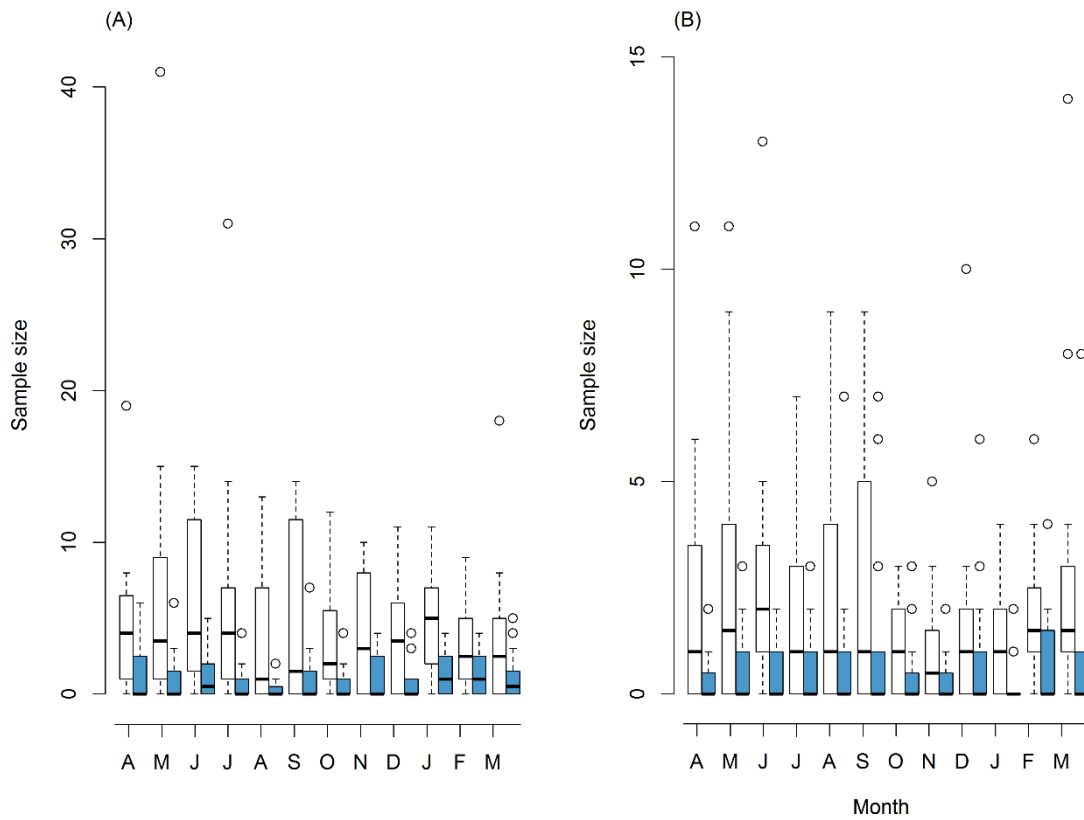


Figure S1. Monthly number of individuals of total sampled foxes (no fill) and infected foxes (blue) from 1994 – 2010. (A) Juveniles; (B) adults. Boxes show the sample median, minimum and maximum. Error bars indicate the lower and upper quartiles and outliers are indicated by open circles.

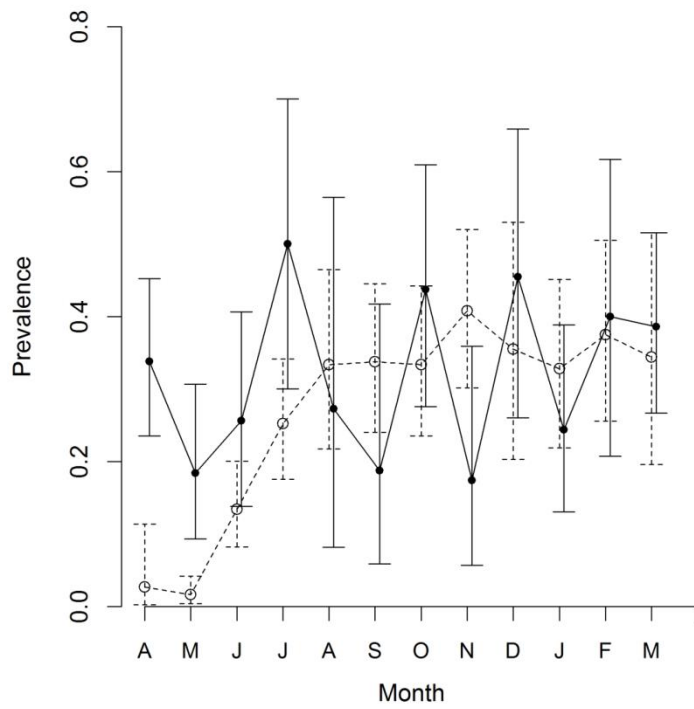


Figure S2. Mean monthly prevalence of mange infection for juveniles (dashed line, open circles) and adults (solid line, closed circles) from 1994 – 2010, with 95% confidence intervals.

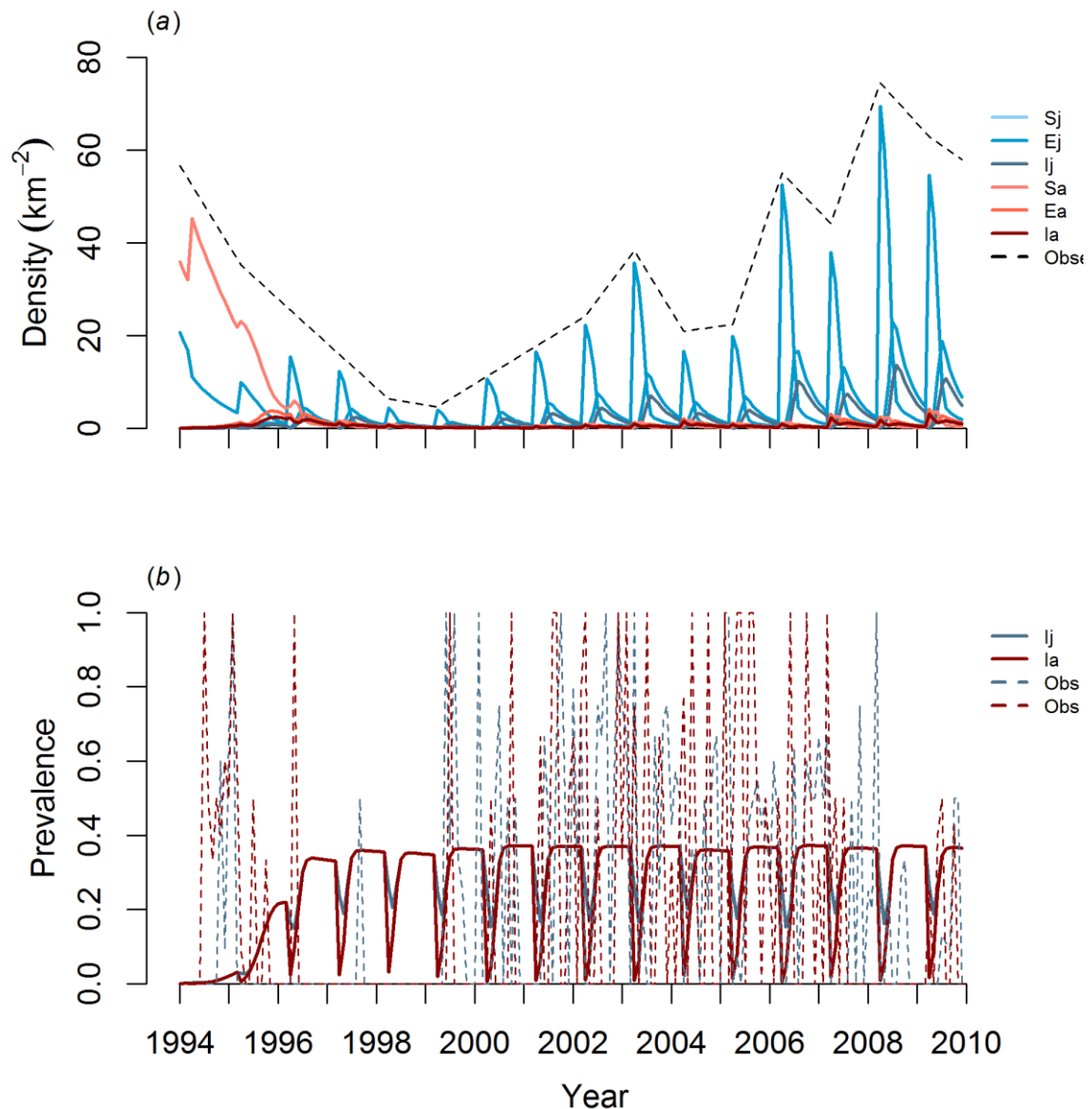


Figure S3. The predicted population density (a) and prevalence (b) for the frequency-dependent SEI model (M_F). Solid lines indicate predicted density for juveniles and adults of susceptible and exposed individuals (S_j , S_a , E_j , E_a) and predicted density and prevalence of infected juveniles and adults (I_j and I_a), against the observed population density and age-specific prevalence data (dashed lines).

Supplementary References

1. Baker P.J., Funk S.M., Harris S., White P.C.L. 2000 Flexible spatial organization of urban foxes, *Vulpes vulpes*, before and during an outbreak of sarcoptic mange. *Anim Behav* **59**, 127-146
2. Soulsbury C.D., Iossa G., Baker P.J., Cole N.C., Funk S.M., Harris S. 2007 The impact of sarcoptic mange *Sarcoptes scabiei* on the British fox *Vulpes vulpes* population. *Mammal Rev* **37**, 278-296.(10.1111/j.1365-2907.2007.00101.x)
3. Whiteside H.M., Dawson D.A., Soulsbury C.D., Harris S. 2011 Mother knows best: dominant females determine offspring dispersal in red foxes (*Vulpes vulpes*). *PLoS ONE* **6**, e22145.(10.1371/journal.pone.0022145)
4. Baker P.J., Newman T.J., Harris S. 2001 Bristol's foxes - 40 years of change. *British Wildlife* **12**, 411-417
5. Newman T.J., Baker P.J., Harris S. 2002 Nutritional condition and survival of red foxes with sarcoptic mange. *Can J Zool* **80**, 154-161.(10.1139/z01-216)
6. Arlian L.G. 1989 Biology, host relations, and epidemiology of *Sarcoptes scabiei*. *Annu Rev Entomol* **34**, 139-161
7. Begon M., Bennett M., Bowers R.G., French N.P., Hazel S.M., Turner J. 2002 A clarification of transmission terms in host-microparasite models: numbers, densities and areas. *Epidemiol Infect* **129**, 147-153
8. Hone J., Donnelly C.A. 2008 Evaluating evidence of association of bovine tuberculosis in cattle and badgers. *J Appl Ecol* **45**, 1660-1666
9. Arlian L.G., Vyszynski-Moher D.L., Pole M.J. 1989 Survival of adults and developmental stages of *Sarcoptes scabiei* var *canis* when off the host. *Exp Appl Acarol* **6**, 181-187
10. Keeling M.J., Rohani P. 2008 *Modeling infectious diseases in humans and animals*. Princeton, New Jersey, Princeton University Press; 408 p.
11. Richards S.A. 2008 Dealing with overdispersed count data in applied ecology. *J Appl Ecol* **45**, 218-227
12. Anderson D.R., Burnham K.P., White G.C. 1994 AIC model selection in overdispersed capture-recapture data *Ecology* **75**, 1780-1793
13. Press W.H., Teukolsky S.A., Vetterling W.T., Flannery B.P. 2007 *Numerical recipes: the art of scientific computing*. 3rd ed. Cambridge, Cambridge University Press; 1256 p.

14. Richards S.A., Whittingham M.J., Stephens P.A. 2011 Model selection and model averaging in behavioural ecology: the utility of the IT-AIC framework. *Behavioral Ecology and Sociobiology* **65**, 77-89.(10.1007/s00265-010-1035-8)
15. Diekmann O., Heesterbeek J.A.P., Metz J.A.J. 1990 On the definition and the computation of the basic reproduction ratio R_0 in models for infectious diseases in heterogeneous populations. *J Math Biol* **28**, 365-382
16. Heffernan J.M., Smith R.J., Wahl L.M. 2005 Perspectives on the basic reproductive ratio. *J Royal Soc Interface* **2**, 281-293
17. van den Driessche P., Watmough J. 2002 Reproduction numbers and sub-threshold endemic equilibria for compartmental models of disease transmission. *Math Biosci Eng* **180**, 29–48
18. Caswell H. 2001 *Matrix population models: construction, analysis, and interpretation*. 2nd ed. Sunderland, Massachusetts, USA, Sinauer Associates; 722 p.
19. Mills L.S. 2007 *Conservation of wildlife populations: demography, genetics, and management*. Oxford, Blackwell; 424 p.
20. Heesterbeek J.A.P. 2002 A brief history of R_0 and a recipe for its calculation. *Acta Biotheor* **50**, 189-204
21. van den Driessche P., Watmough J. 2008 Further notes on the basic reproduction number. *Mathematical Epidemiology* **1945**, 159-178
22. Diekmann O., Heesterbeek J.A.P., Roberts M.G. 2010 The construction of next-generation matrices for compartmental epidemic models. *J Royal Soc Interface* **7**, 873-885
23. Rohani P., Breban R., Stallknecht D.E., Drake J.M. 2009 Environmental transmission of low pathogenicity avian influenza viruses and its implications for pathogen invasion. *Proc Natl Acad Sci USA* **106**, 10365-10369